Internal Variability Increased Arctic Amplification during 1980-2022

Aodhan John Sweeney[1], Qiang Fu[2], Stephen Po-Chedley[3], Hailong Wang[1], and Muyin Wang[3,4]

[1]Affiliation not available
[2]Department of Atmospheric Sciences, University of Washington
[3]Program for Climate Model Diagnosis and Intercomparison, Lawrence Livermore National
[4]Laboratory

October 19, 2023

Internal Variability Increased Arctic Amplification during 1980-2022

Aodhan J. Sweeney[1], Qiang Fu[1], Stephen Po-Chedley[2], Hailong Wang[3], Muyin Wang[4,5]

[1]University of Washington, Department of Atmospheric Sciences
[2]Program for Climate Model Diagnosis and Intercomparison, Lawrence Livermore National Laboratory, Livermore, CA, USA
[3]Atmospheric Sciences and Global Change Division, PNNL
[4]University of Washington, Cooperative Institute for Climate, Ocean, and Ecosystem Studies
[5]Pacific Marine Environmental Laboratory, Oceanic and Atmospheric Research, NOAA

Corresponding authors: Aodhan Sweeney (aodhan@uw.edu) and Qiang Fu (qfu@uw.edu)

Key Points:

- Internally generated and externally forced temperature trends over the Arctic and globe can be partitioned using machine learning methods
- Internal variability has enhanced Arctic warming while damping global warming over 1980-2022
- Accounting for internal variability in observations reconciles discrepancies between simulated and observed Arctic Amplification

Abstract

Since 1980, the Arctic surface has warmed four times faster than the global mean. Enhanced Arctic warming relative to the global average warming is referred to as Arctic Amplification (AA). While AA is a robust feature in climate change simulations, models rarely reproduce the observed magnitude of AA, leading to concerns that models may not accurately capture the response of the Arctic to greenhouse gas emissions. Here, we use CMIP6 data to train a machine learning algorithm to quantify the influence of internal variability in surface air temperature trends over both the Arctic and global domains. Application of this machine learning algorithm to observations reveals that internal variability increases the pace of warming in the Arctic but slows global warming in recent decades, inflating AA since 1980 by 38% relative to the externally forced AA. Accounting for the role of internal variability reconciles the discrepancy between simulated and observed AA.

Plain Language Summary

The Arctic has been warming four times as quickly as the global mean since 1980. This so-called Arctic Amplification (AA) has unprecedented impacts on Arctic environments and livelihoods. AA is robustly simulated by climate models, but simulations rarely reproduce the observed levels of AA for 1980-2022. This may be due to a model misrepresentation of the Arctic's sensitivity to increasing greenhouse gases. Another possibility is that the large, observed value of AA is inflated by natural fluctuations in the climate system. Here, we use machine learning to quantify the contribution of natural fluctuations to observed AA. We show that natural fluctuations have inflated AA by 38%, and thus reconcile model-observation differences and suggest that the observed large AA over 1980 to present would not persist to the future.

1. Introduction

Manabe and Wetherald (1975) first found that the "warming in higher latitudes is magnified two to three times the overall amount" in response to the CO2 increase. This phenomenon was later termed as Arctic Amplification (AA), and has been consistently seen in both model simulations and observations (e.g., Rantanen et al., 2022). From 1980 to 2022 observed surface temperatures in the Arctic (defined here as the region poleward of 70°N) have warmed about four times faster than the global mean (Rantanen et al., 2022; Chylek et al., 2022). Climate models reliably simulate an amplified Arctic warming, but the magnitude of simulated AA is consistently lower than in observations (e.g., England et al., 2021; Hahn et al., 2021; Holland and Landrum, 2021). Many physical processes have been proposed to explain the observed and simulated AA, including both local feedbacks (Manabe and Wetherald, 1975; Holland & Bitz, 2003; Goose et al., 2018; Zhang et al., 2018; Zhang et al., 2020; Feldl et al., 2020; Hahn et al., 2021; England et al., 2021; Zhang et al., 2021) and remote teleconnections (Baxter et al., 2019), yet the relative contribution of each of these processes is not well known (Previdi et al., 2021). Differences between the observed and simulated AA suggests that current climate models may not correctly capture the response of the Arctic and/or global climate to external forcings (Rantanen et al., 2022; Chylek et al., 2022).

The observed and simulated AA differences might also be partly caused by natural, internal climate variability (Rantanen et al., 2022; Chylek et al., 2022), given that certain components of the Arctic (e.g., sea ice) exhibit substantial decadal variations due to internal climate variability (Kay et al., 2011; Stroeve et al., 2012; Swart et al., 2015; Ding et al., 2019;

Olonscheck et al., 2019; Topál et al., 2020; Deser et al., 2020; Wu et al., 2021; Bonan et al., 2021). Arctic sea ice cover trends are tightly coupled to surface temperature, due to strong impacts on albedo and surface heat fluxes (Serreze and Barry 2011; IPCC Chapter 3; Feldl et al., 2020; Deng and Dai., 2022). Due to this coupling, the large internal variability in sea ice likely manifests as changes in Arctic surface temperature. Decadal atmospheric and oceanic internal variability may also contribute to recent Arctic warming (Proshutinsky et al., 2015; Kim and Kim, 2017). Internal variability has also been implicated in the recent slowdown of global warming in the early 21st century (Kosaka and Xie, 2013; Huber & Knutti, 2014; Guan et al 2015). However, it is still an open question whether the large differences in AA between model simulations and observations are mainly caused by climate model deficiencies, internal variability, or both (Rantanen et al., 2022; Chylek et al., 2022).

When comparing the model simulations with observations, it is important to account for the effects of internal variability (Deser et al., 2020). In single-model large ensembles, the same model is run with small perturbations in the initial conditions leading to unique realizations of internal variability in each ensemble member. The externally forced signal can be estimated using the ensemble mean and the internal variability associated with each ensemble member can be obtained as the deviations from this mean (Kay et al., 2015). However, this technique cannot be applied to observations because there is only one observational record. To disentangle the effects of external forcing and internal variability on observed changes in climate, previous work has used various spatiotemporal analysis methods (e.g., Smoliak et al., 2010; Wallace et al., 2012; Deser et al., 2014; Smoliak et al., 2015; Deser et al., 2016; Gong et al., 2019; Guo et al., 2019; Wills et al., 2020; Räisänen, 2020; Po-Chedley et al., 2021; Po-Chedley et al., 2022). Here, we build upon previous methods using a machine learning (ML) approach, which is trained to separate the contribution of external forcing and internal variability to surface warming using climate model large ensembles (see table S1 for information about the model large ensembles). The model-trained ML algorithm is then applied to observations to estimate the relative influence of external forcing and internal variability on recent (1980-2022) Arctic and global surface temperature changes. We find that internal variability enhanced Arctic warming but damped global warming, resulting in amplified AA in the observed record. We show that accounting for the effects of internal variability on Arctic and global surface warming reconciles differences between observed and model-simulated AA.

2. Data and Methods

The magnitude of AA depends on the southern boundary used to define the Arctic (Davy et al., 2018). In this study, AA is defined as the surface air temperature trend for the region poleward of 70°N divided by the global mean trend from 1980-2022. AA is derived from four different observational temperature datasets including the Met Office Hadley Centre/Climatic Research Unit's global surface temperature dataset version 5 (HadCRUTv5), Berkeley Earth Land/Ocean Temperature Record (BerkeleyEarth), GISS Surface Temperature Analysis version 4 (GISTv4), and the NOAA Merged Land Ocean Global Surface Temperature Analysis version 5 (NOAAv5) (Hersbach et al., 2020; Morice et al., 2021; Rhode & Hausfather., 2020; Lenssen et al., 2019; Zhang et al., 2019). Fig. S1 indicates that warming is amplified north of 70ºN in all four observational datasets.

Following recent work showing that ML methods can effectively isolate internally generated and externally forced trends (Barnes et al., 2019; Gordon and Barnes, 2022; Po-

Chedley et al., 2022; Connolly et al., 2023), we create ML algorithms to isolate these trend contributions in observed surface air temperature during the 43-year period from 1980-2022 over both the Arctic and globe. To do this, we create a training dataset based on 10 CMIP6 models, of which each have at least 10 ensemble members (Table S1). Aside from the CESM2 large ensemble from the CMIP6 archive, we also include the 50 member CESM2 large ensemble with updated biomass burning aerosol emissions that better represents the historical radiative forcings in the high latitude northern hemisphere (referred to here as CESM2_SBMB) (Rodgers et al., 2021; Fasullo et al., 2022). The target data in our training are the externally forced and internally generated surface air temperature trends averaged over a given region (either Arctic or globe), which are derived as the mean trend and deviation from the mean in each ensemble. These trends are calculated using 43-year periods separated by five years spanning 1900-2047 (i.e., 1900-1942, 1905-1947, …, 1980-2022, …, 2005-2047). CMIP6 and CESM2_SBMB historical runs end in 2014, so we extend these simulations using either SSP3-7.0 or SSP5-8.5 (O'Neill et al, 2016) until 2047[1] for seven of the models in our training data. The remaining four models only have sufficient ensemble members until 2014, and thus only periods from 1900-2012 are used to train our ML algorithm for these models. The ML algorithm is trained using 10 models with large ensembles but with one model leftout (see more details below). We test the results from 1980-2022 using the leftout model that is one of seven with extensions beyond 2014 (Table S1). The observationally derived AAs are compared with the seven large ensembles for 1980-2022, and with all other CMIP6 models with data available over 1980-2022 (OthersAllEM), even though each of them does not have enough ensemble members to properly derive the externally forced AA.

The predictor data (i.e., the input used to estimate the targets) are maps of surface air temperature (SAT) and sea level pressure (SLP) trends. Our ML pipeline is thus designed to accept 43- year trend maps of both SAT and SLP and returns the components of the trend averaged over the Arctic or globe due to internal variability and external forcing. All maps of SAT and SLP trends are regridded to a common 2.5°x2.5° grid. The ML algorithms are trained for the predictions of the Arctic and global cases separately. For the global case, input data are global trend maps of SLP and SAT. For the Arctic case, we only use trend maps poleward of 20°N (Wallace et al., 2012; Smoliak et al., 2015). Patterns of surface temperature changes can impact both regional and global scale warming and can provide information about the relative role of internal variability (Dong et al., 2019; Dong et al., 2020). Outside the tropics SLP can be used as a proxy for the atmospheric circulation (Smoliak et al., 2010; Deser et al., 2014) and has been used to isolate dynamically induced changes in surface temperature in the northern hemisphere (Wallace et al., 2012; Guan et al., 2015). Further, using more than one geophysical variable may help in identifying signals of external forcing (Rader et al., 2022).

We use the convolutional neural networks (CNNs) that are trained separately for the Arctic and global-mean temperature trends (see Text S1). We validate the skill of the CNN using a leave-one-out cross validation, where the CNN is trained on data from all models except the model we test on (which is one of seven models covering 1900-2047) (see Text S1). This prohibits the CNN from learning model specific biases. When applying the CNN to the out-of-sample large ensemble, we also apply it to observed SAT and SLP trend patterns to derive the externally and internally generated trends. SAT trends are those of the four observational datasets from 1980-2022. SLP trends are from the ERA5, MERRA-2, and JRA-55 reanalysis

[1] SSP5-8.5 is used when both are available.

datasets over the same time period (see Fig. S2 for a comparison of SLP trends between reanalyses used and the 20th century reanalysis for 1980-2015, showing a good agreement). Because we have four SAT datasets and three SLP datasets, in total we have 12 sets of SAT and SLP trend maps. For each of the seven models that we test on during the cross validation, we get estimates of internally generated and externally forced trends from each of the 12 observational SAT and SLP sets, providing 84 estimates of the internally generated and externally forced trends. The central value is then the mean over all 84 observational predictions and the uncertainty is quantified by taking into account both observational and ML prediction uncertainties (Text S2).

3. Arctic Amplification in Observations and CMIP6

Fig. 1A shows the patterns of local amplification over the northern hemisphere high latitudes from the observational mean and multi-model mean (MMM). Observations show maximum amplification poleward of 70°N and that large extents of the Arctic Ocean have warmed at least four times as quickly as the global mean. Local amplification ratios exceed six in the Barents Sea, consistent with strong reductions in sea ice concentration in the same region (Screen & Simmons, 2010; Isaksen et al., 2022; Parkinson, 2022). Although the MMM exhibits a similar pattern of local amplification, it substantially underestimates the magnitude as compared to observations (Ye & Messori, 2021; Rantanen et al., 2022).

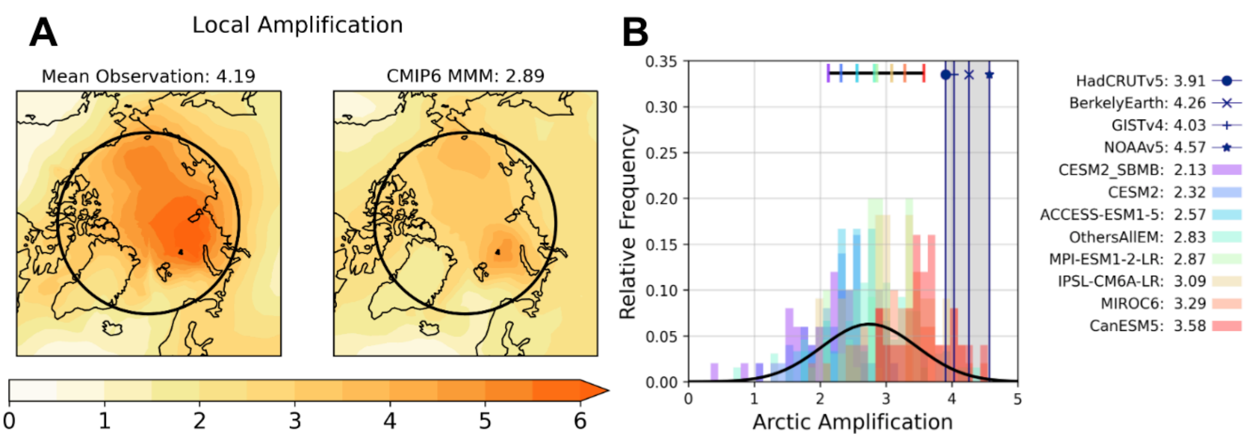

Fig 1: (**A**) Local amplification (i.e., local surface air temperature trend divided by global mean temperature trend) over the northern high latitudes from the average of observational datasets and the multi-model mean during 1980 to 2022. The Arctic is the region poleward of 70°N (black circle), and the corresponding Arctic Amplification (AA) (i.e., the Arctic mean temperature trend divided by global mean trend) is provided at the top of each plot. (**B**) Comparisons of AA in observations and CMIP6 models. Observations are shown using vertical lines, and grey shading shows their range. Histograms show the relative frequency distribution of AA over 1980-2022 for each model, which is normalized by its number of ensemble members. The black curve shows a normal distribution fitted to all model AA values. The black horizontal line shows the range of forced AAs and the vertical tick marks represent the ensemble-mean AA for each model. The values of AA from each observation and forced AA from each model are provided in the legend.

Figure 1B shows the AA from the four observational datasets and seven large ensembles and OthersAllEM (see section 2) for 1980-2022. While the forced component of AA ranges from

2.13 to 3.58 across models, individual ensemble members span a much larger range (Fig. S3 shows each large ensembles AA distribution indivisually). Since the forcing is the same for all members of each model large ensemble, the deviations from the forced AA for a given ensemble member is entirely due to internal variability (OthersAllEM is an exception for which the deviations could also be partly due to differences in forced trends). While the magnitude of AA varies across the observations, all show extreme AA compared to the distribution of model simulations (Fig. 1B). All observational AA estimates sit outside the range of forced AA predicted by the large ensembles (i.e., outside the range of the horizontal black bar), and AA from NOAA Global Temperature v5 (4.57) exceeds AA from all model ensemble members. Observationally derived AA is weakest in HadCRUTv5 (3.91), which still exceeds 94% of the simulated AAs in Fig. 1B.

The exceptionally high AA in observations compared to model simulations could be due to systematic model biases in the representation of internal variability, biases in the simulated response to external forcing, biases in the prescribed model forcing, or the observed AA being an extremely unlikely event (Rantanen et al., 2022). Because AA is defined as the trend poleward of 70°N divided by the global mean, biases in either the Arctic or global warming would impact the comparison of AA. To investigate how well models simulate global and Arctic warming individually, Fig. 2 shows the distribution of Arctic and global warming in observations and model simulations (Figs. S4 and S5 show each large ensemble trend distribution individually over the Arctic and globe, respectively). Simulations of Arctic warming exhibit a very large range of trends from nearly 0 up to 2 K/decade for 1980-2022. Although a significant amount of this spread is due to differences between models (e.g., compare forced trends from CanESM5 to those from all other models), even individual models have Arctic warming trends that vary by ±0.5 K/decade due to internal variability (see, e.g., ACCESS-ESM1-5 in Fig. S4). The observed Arctic warming ranges from 0.742 to 0.835 K/decade from the four observational datasets, with a mean of 0.791 K/decade, which are all well within the range of Arctic warming predicted by models (Fig. 2A). Thus, the observed Arctic warming is not as extreme as AA when compared to model simulations.

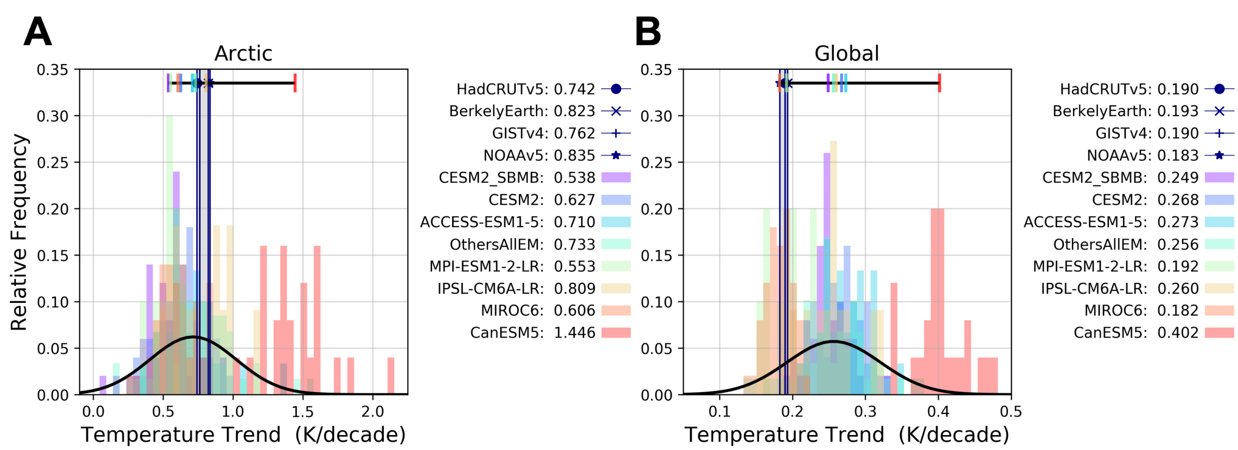

Fig 2: Surface air temperature trends over 1980-2022 for the (A) Arctic and (B) global mean. The histograms show the distributions from model simulations, and the vertical lines represent the observations where grey shading shows their range. The black curve shows a normal distribution fitted to all the simulated temperature trends. The horizontal black line shows the range of externally forced trends with ticks showing individual models' forced trends. The trend

values from individual observational datasets and forced trend values from individual models are provided in the legend.

The global warming trend from the four observational datasets ranges from 0.183 to 0.193 K/decade with a mean of 0.189 K/decade, which is on the lower side of the simulated range of externally forced trends (Fig. 2B). However, some models have ensemble members that simulate global warming trends below what is observed, suggesting that internal variability may damp the rate of global warming (Kosaka and Xie, 2013; Watanabe et al., 2014; Zhang et al., 2016; Xie & Kosaka, 2017; Wu et al., 2019). Next, we attempt to partition the observed Arctic and global warming trends into their externally and internally generated components.

4. Separating Internal Generated and Externally Forced Trends in Observations

The test of the CNN algorithms on each of the seven models for 1980-2022 are shown as scatter points in Fig. 3, which suggest that when presented with a set of SAT and SLP trend maps from a model ensemble not used during training, the CNN can reliably separate the internal and external contributions to the trends averaged over the Arctic and globe. This is despite the wide range of internally generated and externally forced trends simulated by models (see Fig. 2). The skill of the CNN results from its ability to learn the patterns (in SAT and SLP) that correspond with the internally generated and external forced trends in both the Arctic and global domains. The CNN also generalizes well to simulations with forced trends far from the MMM (e.g., red dots showing results for CanESM5 in Fig. 3B, E). Although the CNN predicts the internal and external trends separately, their sum accurately reproduces the total trend (see Fig. 3C and 3F). This conservation of the total trend is not explicitly targeted during training but arises from learning this closure in the training data.

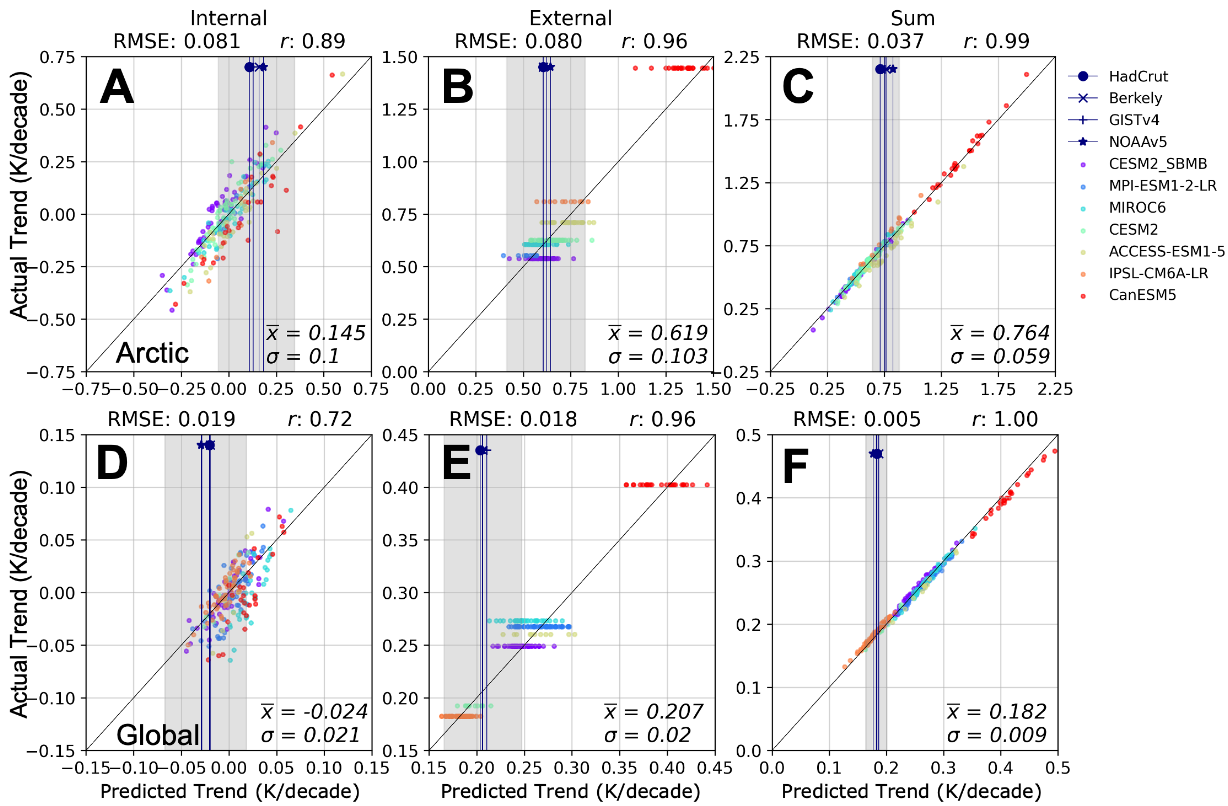

Fig 3: (A-C) Arctic and (D-F) global surface air temperature trends predicted from the CNN (x-axis) versus corresponding actual trends (y-axis) over 1980-2022. The root mean squared error (RMSE) and correlation coefficient (r) are shown at the top of each plot. (A, D) shows results for internally generated trends, (B, E) shows the externally forced trends, and (C, F) shows the sum of the internally generated and externally forced trends. The vertical lines show the mean observational estimate for each temperature record, and the grey shading shows the ± 2σ uncertainty of mean prediction. The mean (x̄) and its standard deviation (σ) based on observations are provided in the bottom right of each plot. The black diagonal line in (A-F) is the 1:1 line.

Having shown that the CNNs can reliably predict the internal and external trends in models, we apply the CNNs to observations from 1980-2022 using the four SAT datasets and three SLP datasets. The mean results for each SAT dataset are shown by the vertical lines in Fig. 3 with the 2σ confidence interval (Text S2) for the mean of all observational datasets. Predictions based on observational datasets indicate that internal variability has enhanced Arctic surface warming over 1980-2022 by 0.145 K/decade (Fig. 3A). The CNN predicts that the externally generated Arctic surface temperature trend is 0.619 K/decade. This suggests that internal variability has accelerated the pace of Arctic warming by ~23% relative to the forced trend. Using all ensembles from the 7 models for all 43-year periods separated by 5-year increment over 1900-2047/2012, the 2σ spread of Arctic internal variability is ±0.324 K/decade. Many studies have shown that surface temperature trends in the Arctic are strongly coupled to sea ice trends, and that recent declines in sea ice cover have been enhanced by multidecadal variability (Serreze et al., 2009; Screen and Simmons, 2010; Kay et al., 2011; Ding et al., 2019; Deng and Dai, 2022). Our results agree with previous studies showing that internal variability is an important contribution to recent trends in Arctic climate change (Ding et al., 2019; Bonan et al., 2019; Chylek et al., 2022).

Application of the CNN to the global case suggests that internal variability dampens the observed temperature trend, which is also consistent with previous studies (Kosaka and Xie, 2013; Xie and Kosaka, 2017; Tokarska et al., 2020; Po-Chedley et al., 2022). All observational estimates show that internal variability reduces global surface warming over 1980-2022, with a central estimate of -0.024 K/decade (Fig. 3D). The global CNN predicts the externally generated trend to be 0.207 K/decade. This suggests that internal variability has damped the global warming by ~12% relative to the forced trend since 1980. Although this internal variability is substantial, the 2σ spread of internal variability from all large ensembles over the 1900-2047/2012 period is ±0.051 K/decade.

5. Implications for Arctic Amplification and Discussions

Internal variability can impact AA through its effect on Arctic warming, global warming, or both. ML algorithms applied here can partition the contribution of externally forced and internally generated trends both over the Arctic and over the globe. Application of these algorithms to observations suggests that internal variability has enhanced Arctic surface warming (+0.145 K/decade) while simultaneously dampening global mean surface warming (-0.024 K/decade) over 1980-2022 (Figs. 3A&D). Because AA is the surface temperature trend in the Arctic divided by the global mean trend, the opposing role of internal variability in the Arctic and global average inflates observed AA. Figure 4 is the same as Fig. 1B but with AA estimates after we first subtract the contribution of internal variability derived form ML algoriths from both the Arctic and global mean trends and then recalculate their ratio. This was done for both observations and each ensemble member of the seven large ensembles (Fig. S6 shows each large ensembles distribution of AA after removing internal variability indivisually). Upon removing the estimated effect of internal variability from the Arctic and global mean surface air temperature trend, AA from climate model simulations and observational datasets exhibit excellent agreement (c.f, Fig. 4 to Fig. 1B).

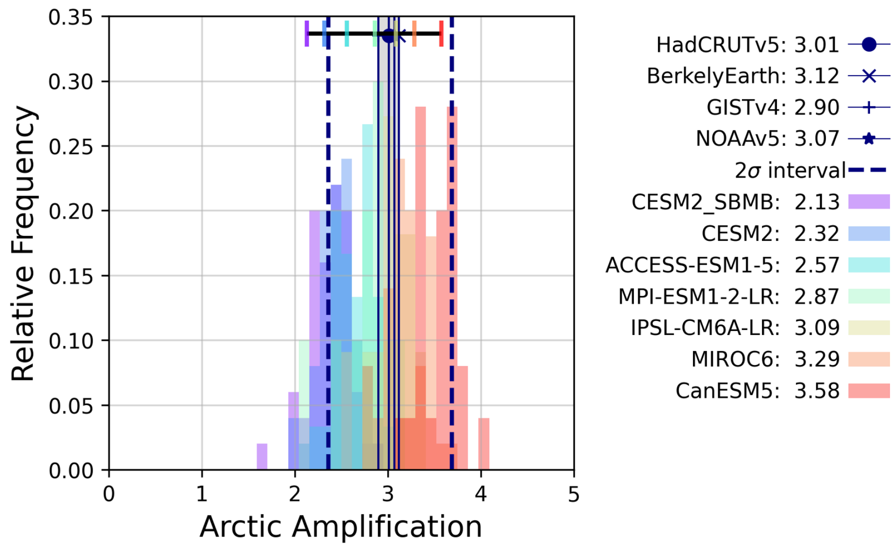

Fig. 4: Same as Fig. 1 (B) but showing the AA estimates after subtracting the contributions of internal variability, as derived from the ML algorithms, from Arctic and global warming. This was done for both observations and each ensemble member of the seven large ensembles. The vertical blue dashed lines show the 2σ range of the estimated forced AA based on observations.

After subtracting the internally generated trend from the mean observational trend over the Arctic (0.791 K/decade) and globe (0.189 K/decade), the externally generated trend is estimated as 0.646 K/decade and 0.213 K/decade, respectively, meaning that the externally forced AA is 3.03. A similar result is obtained by using the externally forced Arctic to global warming trends directly estimated by the CNN, which are 0.619 K/decade and 0.207 K/decade (Figs. 3B&E), and the resulting externally forced AA is 2.99. Our results shown here suggest that internal variability plays a substantial role in inflating recent AA and increased the 1980-2022 AA by 38%. Key to this result, is recognizing that internal variability has enhanced Arctic warming while simultaneously damping global warming. Vertical blue dashed lines show the 2σ spread of externally forced AA based on observations (see Text S2). Figure 4 shows that the estimates of observed, externally forced AA is still within the range of forced AA based on model simulations even when this uncertainty is included. Although here we present results using a definition of the Arctic as poleward of 70°N, repeating the analysis by defining the Arctic as poleward of 60°N produces similar results (see Fig. S7). This study uses CNNs (Text S1 and Fig. S8) instead of linear pattern matching algorithms, e.g., Partial Least Squares regression (PLS) (Po-Chedley et al., 2022), because CNNs better minimize the MSE, but results are similar using either CNNs or PLS methods (see Fig. S9 and S10). The mean AA ratio after removing internal variability contributions to observed trends based on PLS regression and the CNN is 2.98 and 3.03, respectively.

Although we stress internal variability's role in inflating recent AA, these results do not discount the possible influence of forcing on the simulated-versus-observed differences in AA. Systematic biases in the forcing prescription can have a significant impact on simulated AA during 1980-2022. For example, changes in the amount of biomass burning prescribed in CESM2_SBMB compared to CESM2 lead to decreased surface warming in the Northern Hemisphere high latitudes and thus a smaller AA ratio in CESM2_SBMB (Fig. 1B). Because AA is defined as the ratio of the total Arctic and global warming, a forcing bias in either region will impact the magnitude of AA even if internally generated trends match observations. Given that the externally forced and internally generated trends estimated from observations are within the bounds of the simulated externally forced and internally generated trends in the large ensembles, a pertinent question is why don't more models simulate the observed levels of AA? Crucial to reproducing the observed AA is simulating internal variability that enhances Arctic warming while simultaneously dampening global warming. The fact that model simulations generally do not reproduce the observed levels of AA may suggest that while models during the 1980-2022 period can simulate the observed amplitude of internal variability in the Arctic and over the globe separately, they struggle to simulate the combined manifestation of internal variability that enhances Arctic warming while suppressing global warming (Rosenblum & Eisenman, 2017; Rantanen et al., 2022). Our machine learning schemes work well partly because they are trained separately for the Arctic and global-mean temperature trends. Our results show that considering internal variability can reconcile the discrepancy between observed and simulated AA but also calls for the need to better understand this unusual manifestation of internal variability.

Acknowledgments

This research was supported by the U.S. Department of Energy (DOE), Office of Science, Office of Biological and Environmental Research, Regional and Global Model Analysis (RGMA) program area, as part of the HiLAT-RASM project. This research was also supported by the NASA FINESST Grant 80NSSC22K1438 and NSF Grant AGS-2202812. Additional funding was provided by the Calvin Professorship in Atmospheric Sciences. S.P.-C was supported through the PCMDI Project, which is funded by the RGMA program area of the Office of Science at DOE. M. Wang is funded with support of the Arctic Research Program of the NOAA Global Ocean Monitoring and Observing (GOMO) office through the Cooperative Institute for Climate, Ocean, & Ecosystem Studies (CICOES) under NOAA Cooperative Agreement NA20OAR4320271, Contribution No 2023-1295, and Pacific Marine Environmental Laboratory Contribution No 5531. Research at Lawrence Livermore National Laboratory was performed under the auspices of U.S. DOE Contract DE-AC52-07NA27344. The Pacific Northwest National Laboratory (PNNL) is operated for DOE by Battelle Memorial Institute under contract DE-AC05-76RLO1830. We would like to acknowledge high-performance computing support from Cheyenne (doi:10.5065/D6RX99HX) provided by NCAR's Computational and Information Systems Laboratory, sponsored by the National Science Foundation, for the analyses presented in this study and for data management, storage, and preservation.

Open Research

Data used in this study is stored at https://zenodo.org/record/8286633. Code required to recreate the results is provided at https://github.com/AodhanSweeney/AA_InternalExternalPartitioning.

References

Barnes, E. A., Hurrell, J. W., Ebert-Uphoff, I., Anderson, C., & Anderson, D. (2019). Viewing Forced Climate Patterns Through an AI Lens. *Geophysical Research Letters*, *46*(22), 13389–13398. https://doi.org/10.1029/2019GL084944

Baxter, I., Ding, Q., Schweiger, A., L'Heureux, M., Baxter, S., Wang, T., et al. (2019). How Tropical Pacific Surface Cooling Contributed to Accelerated Sea Ice Melt from 2007 to 2012 as Ice Is Thinned by Anthropogenic Forcing. *Journal of Climate*, *32*(24), 8583–8602. https://doi.org/10.1175/JCLI-D-18-0783.1

Bonan, D. B., Lehner, F., & Holland, M. M. (2021). Partitioning uncertainty in projections of Arctic sea ice. *Environmental Research Letters*, *16*(4), 044002. https://doi.org/10.1088/1748-9326/abe0ec

Chapter 3: Polar regions — Special Report on the Ocean and Cryosphere in a Changing Climate. (n.d.). Retrieved June 10, 2023, from https://www.ipcc.ch/srocc/chapter/chapter-3-2/

Chattopadhyay, A., Hassanzadeh, P., & Pasha, S. (2020). Predicting clustered weather patterns: A test case for applications of convolutional neural networks to spatio-temporal climate data. *Scientific Reports*, *10*(1), 1317. https://doi.org/10.1038/s41598-020-57897-9

Chylek, P., Folland, C., Klett, J. D., Wang, M., Hengartner, N., Lesins, G., & Dubey, M. K. (2022). Annual Mean Arctic Amplification 1970–2020: Observed and Simulated by CMIP6 Climate Models. *Geophysical Research Letters*, *49*(13), e2022GL099371. https://doi.org/10.1029/2022GL099371

Connolly, C., Barnes, E. A., Hassanzadeh, P., & Pritchard, M. (2023). Using Neural Networks to Learn the Jet Stream Forced Response from Natural Variability. *Artificial Intelligence for the Earth Systems*, *2*(2). https://doi.org/10.1175/AIES-D-22-0094.1

Davy, R., Chen, L., & Hanna, E. (2018). Arctic amplification metrics. *International Journal of Climatology*, *38*(12), 4384–4394. https://doi.org/10.1002/joc.5675

Deng, J., & Dai, A. (2022). Sea ice–air interactions amplify multidecadal variability in the North Atlantic and Arctic region. *Nature Communications*, *13*(1), 2100. https://doi.org/10.1038/s41467-022-29810-7

Deser, C., Lehner, F., Rodgers, K. B., Ault, T., Delworth, T. L., DiNezio, P. N., et al. (2020). Insights from Earth system model initial-condition large ensembles and future prospects. *Nature Climate Change*, *10*(4), 277–286. https://doi.org/10.1038/s41558-020-0731-2

Deser, Clara, Phillips, A. S., Alexander, M. A., & Smoliak, B. V. (2014). Projecting North American Climate over the Next 50 Years: Uncertainty due to Internal Variability. *Journal of Climate*, *27*(6), 2271–2296. https://doi.org/10.1175/JCLI-D-13-00451.1

Deser, Clara, Terray, L., & Phillips, A. S. (2016). Forced and Internal Components of Winter Air Temperature Trends over North America during the past 50 Years: Mechanisms and Implications. *Journal of Climate*, *29*(6), 2237–2258. https://doi.org/10.1175/JCLI-D-15-0304.1

Ding, Q., Schweiger, A., L'Heureux, M., Steig, E. J., Battisti, D. S., Johnson, N. C., et al. (2019). Fingerprints of internal drivers of Arctic sea ice loss in observations and model simulations. *Nature Geoscience*, *12*(1), 28–33. https://doi.org/10.1038/s41561-018-0256-8

Dong, Y., Proistosescu, C., Armour, K. C., & Battisti, D. S. (2019). Attributing Historical and Future Evolution of Radiative Feedbacks to Regional Warming Patterns using a Green's Function Approach: The Preeminence of the Western Pacific. *Journal of Climate*, *32*(17), 5471–5491. https://doi.org/10.1175/JCLI-D-18-0843.1

Dong, Y., Armour, K. C., Zelinka, M. D., Proistosescu, C., Battisti, D. S., Zhou, C., & Andrews, T. (2020). Intermodel Spread in the Pattern Effect and Its Contribution to Climate Sensitivity in CMIP5 and CMIP6 Models. *Journal of Climate*, *33*(18), 7755–7775. https://doi.org/10.1175/JCLI-D-19-1011.1

England, M. R., Eisenman, I., Lutsko, N. J., & Wagner, T. J. W. (2021). The Recent Emergence of Arctic Amplification. *Geophysical Research Letters*, *48*(15), e2021GL094086. https://doi.org/10.1029/2021GL094086

Fasullo, J. T., Lamarque, J.-F., Hannay, C., Rosenbloom, N., Tilmes, S., DeRepentigny, P., et al. (2022). Spurious Late Historical-Era Warming in CESM2 Driven by Prescribed Biomass Burning Emissions. *Geophysical Research Letters*, *49*(2), e2021GL097420. https://doi.org/10.1029/2021GL097420

Gong, H., Wang, L., Chen, W., & Wu, R. (2019). Attribution of the East Asian Winter Temperature Trends During 1979–2018: Role of External Forcing and Internal Variability. *Geophysical Research Letters*, *46*(19), 10874–10881. https://doi.org/10.1029/2019GL084154

Goosse, H., Kay, J. E., Armour, K. C., Bodas-Salcedo, A., Chepfer, H., Docquier, D., et al. (2018). Quantifying climate feedbacks in polar regions. *Nature Communications*, *9*(1), 1919. https://doi.org/10.1038/s41467-018-04173-0

Gordon, E. M., & Barnes, E. A. (2022). Incorporating Uncertainty Into a Regression Neural Network Enables Identification of Decadal State-Dependent Predictability in CESM2. *Geophysical Research Letters*, *49*(15), e2022GL098635. https://doi.org/10.1029/2022GL098635

Guan, X., Huang, J., Guo, R., & Lin, P. (2015). The role of dynamically induced variability in the recent warming trend slowdown over the Northern Hemisphere. *Scientific Reports*, *5*(1), 12669. https://doi.org/10.1038/srep12669

Guo, R., Deser, C., Terray, L., & Lehner, F. (2019). Human Influence on Winter Precipitation Trends (1921–2015) over North America and Eurasia Revealed by Dynamical Adjustment. *Geophysical Research Letters*, *46*(6), 3426–3434. https://doi.org/10.1029/2018GL081316

Hahn, L. C., Armour, K. C., Zelinka, M. D., Bitz, C. M., & Donohoe, A. (2021). Contributions to Polar Amplification in CMIP5 and CMIP6 Models. *Frontiers in Earth Science*, *9*. Retrieved from https://www.frontiersin.org/articles/10.3389/feart.2021.710036

Hersbach, H., Bell, B., Berrisford, P., Hirahara, S., Horányi, A., Muñoz-Sabater, J., et al. (2020). The ERA5 global reanalysis. *Quarterly Journal of the Royal Meteorological Society*, *146*(730), 1999–2049. https://doi.org/10.1002/qj.3803

Holland, M. M., & Bitz, C. M. (2003). Polar amplification of climate change in coupled models. *Climate Dynamics*, *21*(3), 221–232. https://doi.org/10.1007/s00382-003-0332-6

Holland, Marika M., & Landrum, L. (2021). The Emergence and Transient Nature of Arctic Amplification in Coupled Climate Models. *Frontiers in Earth Science*, *9*. Retrieved from https://www.frontiersin.org/articles/10.3389/feart.2021.719024

Huber, M., & Knutti, R. (2014). Natural variability, radiative forcing and climate response in the recent hiatus reconciled. *Nature Geoscience*, *7*(9), 651–656. https://doi.org/10.1038/ngeo2228

Isaksen, K., Nordli, Ø., Ivanov, B., Køltzow, M. A. Ø., Aaboe, S., Gjelten, H. M., et al. (2022). Exceptional warming over the Barents area. *Scientific Reports*, *12*(1), 9371. https://doi.org/10.1038/s41598-022-13568-5

Kay, J. E., Deser, C., Phillips, A., Mai, A., Hannay, C., Strand, G., et al. (2015). The Community Earth System Model (CESM) Large Ensemble Project: A Community Resource for Studying Climate Change in the Presence of Internal Climate Variability. *Bulletin of the American Meteorological Society*, *96*(8), 1333–1349. https://doi.org/10.1175/BAMS-D-13-00255.1

Kay, Jennifer E., Holland, M. M., & Jahn, A. (2011). Inter-annual to multi-decadal Arctic sea ice extent trends in a warming world. *Geophysical Research Letters*, *38*(15). https://doi.org/10.1029/2011GL048008

Kim, H.-M., & Kim, B.-M. (2017). Relative Contributions of Atmospheric Energy Transport and Sea Ice Loss to the Recent Warm Arctic Winter. *Journal of Climate*, *30*(18), 7441–7450. https://doi.org/10.1175/JCLI-D-17-0157.1

Kravtsov, S., Grimm, C., & Gu, S. (2018). Global-scale multidecadal variability missing in state-of-the-art climate models. *Npj Climate and Atmospheric Science*, *1*(1), 1–10. https://doi.org/10.1038/s41612-018-0044-6

Lenssen, N. J. L., Schmidt, G. A., Hansen, J. E., Menne, M. J., Persin, A., Ruedy, R., & Zyss, D. (2019). Improvements in the GISTEMP Uncertainty Model. *Journal of Geophysical Research: Atmospheres*, *124*(12), 6307–6326. https://doi.org/10.1029/2018JD029522

Manabe, S., & Wetherald, R. T. (1975). The Effects of Doubling the CO2 Concentration on the climate of a General Circulation Model. *Journal of the Atmospheric Sciences*, *32*(1), 3–15. https://doi.org/10.1175/1520-0469(1975)032<0003:TEODTC>2.0.CO;2

Morice, C. P., Kennedy, J. J., Rayner, N. A., Winn, J. P., Hogan, E., Killick, R. E., et al. (2021). An Updated Assessment of Near-Surface Temperature Change From 1850: The HadCRUT5

Data Set. *Journal of Geophysical Research: Atmospheres*, *126*(3), e2019JD032361. https://doi.org/10.1029/2019JD032361

Olonscheck, D., Mauritsen, T., & Notz, D. (2019). Arctic sea-ice variability is primarily driven by atmospheric temperature fluctuations. *Nature Geoscience*, *12*(6), 430–434. https://doi.org/10.1038/s41561-019-0363-1

O’Neill, B. C., Tebaldi, C., van Vuuren, D. P., Eyring, V., Friedlingstein, P., Hurtt, G., et al. (2016). The Scenario Model Intercomparison Project (ScenarioMIP) for CMIP6. *Geoscientific Model Development*, *9*(9), 3461–3482. https://doi.org/10.5194/gmd-9-3461-2016

Parkinson, C. L. (2022). Arctic sea ice coverage from 43 years of satellite passive-microwave observations. *Frontiers in Remote Sensing*, *3*. Retrieved from https://www.frontiersin.org/articles/10.3389/frsen.2022.1021781

Po-Chedley, S., Santer, B. D., Fueglistaler, S., Zelinka, M. D., Cameron-Smith, P. J., Painter, J. F., & Fu, Q. (2021). Natural variability contributes to model–satellite differences in tropical tropospheric warming. *Proceedings of the National Academy of Sciences*, *118*(13), e2020962118. https://doi.org/10.1073/pnas.2020962118

Po-Chedley, S., Fasullo, J. T., Siler, N., Labe, Z. M., Barnes, E. A., Bonfils, C. J. W., & Santer, B. D. (2022). Internal variability and forcing influence model–satellite differences in the rate of tropical tropospheric warming. *Proceedings of the National Academy of Sciences*, *119*(47), e2209431119. https://doi.org/10.1073/pnas.2209431119

Previdi, M., Smith, K. L., & Polvani, L. M. (2021). Arctic amplification of climate change: a review of underlying mechanisms. *Environmental Research Letters*, *16*(9), 093003. https://doi.org/10.1088/1748-9326/ac1c29

Proshutinsky, A., Dukhovskoy, D., Timmermans, M.-L., Krishfield, R., & Bamber, J. L. (2015). Arctic circulation regimes. *Philosophical Transactions of the Royal Society A: Mathematical, Physical and Engineering Sciences*, *373*(2052), 20140160. https://doi.org/10.1098/rsta.2014.0160

Rader, J. K., Barnes, E. A., Ebert-Uphoff, I., & Anderson, C. (2022). Detection of Forced Change Within Combined Climate Fields Using Explainable Neural Networks. *Journal of Advances in Modeling Earth Systems*, *14*(7), e2021MS002941. https://doi.org/10.1029/2021MS002941

Räisänen, J. (2021). Effect of atmospheric circulation on surface air temperature trends in years 1979–2018. *Climate Dynamics*, *56*(7), 2303–2320. https://doi.org/10.1007/s00382-020-05590-y

Rantanen, M., Karpechko, A. Y., Lipponen, A., Nordling, K., Hyvärinen, O., Ruosteenoja, K., et al. (2022). The Arctic has warmed nearly four times faster than the globe since 1979. *Communications Earth & Environment*, *3*(1), 1–10. https://doi.org/10.1038/s43247-022-00498-3

Rodgers, K. B., Lee, S.-S., Rosenbloom, N., Timmermann, A., Danabasoglu, G., Deser, C., et al. (2021). Ubiquity of human-induced changes in climate variability. *Earth System Dynamics*, *12*(4), 1393–1411. https://doi.org/10.5194/esd-12-1393-2021

Rohde, R. A., & Hausfather, Z. (2020). The Berkeley Earth Land/Ocean Temperature Record. *Earth System Science Data*, *12*(4), 3469–3479. https://doi.org/10.5194/essd-12-3469-2020

Rosenblum, E., & Eisenman, I. (2017). Sea Ice Trends in Climate Models Only Accurate in Runs with Biased Global Warming. *Journal of Climate*, *30*(16), 6265–6278. https://doi.org/10.1175/JCLI-D-16-0455.1

Screen, J. A., & Simmonds, I. (2010). The central role of diminishing sea ice in recent Arctic temperature amplification. *Nature*, *464*(7293), 1334–1337. https://doi.org/10.1038/nature09051

Serreze, M. C., Barrett, A. P., Stroeve, J. C., Kindig, D. N., & Holland, M. M. (2009). The emergence of surface-based Arctic amplification. *The Cryosphere*, *3*(1), 11–19. https://doi.org/10.5194/tc-3-11-2009

Serreze, Mark C., & Barry, R. G. (2011). Processes and impacts of Arctic amplification: A research synthesis. *Global and Planetary Change*, *77*(1), 85–96. https://doi.org/10.1016/j.gloplacha.2011.03.004

Smoliak, B. V., Wallace, J. M., Stoelinga, M. T., & Mitchell, T. P. (2010). Application of partial least squares regression to the diagnosis of year-to-year variations in Pacific Northwest snowpack and Atlantic hurricanes. *Geophysical Research Letters*, *37*(3). https://doi.org/10.1029/2009GL041478

Smoliak, B. V., Wallace, J. M., Lin, P., & Fu, Q. (2015). Dynamical Adjustment of the Northern Hemisphere Surface Air Temperature Field: Methodology and Application to Observations. *Journal of Climate*, *28*(4), 1613–1629. https://doi.org/10.1175/JCLI-D-14-00111.1

Stroeve, J. C., Kattsov, V., Barrett, A., Serreze, M., Pavlova, T., Holland, M., & Meier, W. N. (2012). Trends in Arctic sea ice extent from CMIP5, CMIP3 and observations. *Geophysical Research Letters*, *39*(16). https://doi.org/10.1029/2012GL052676

Swart, N. C., Fyfe, J. C., Hawkins, E., Kay, J. E., & Jahn, A. (2015). Influence of internal variability on Arctic sea-ice trends. *Nature Climate Change*, *5*(2), 86–89. https://doi.org/10.1038/nclimate2483

Topál, D., Ding, Q., Mitchell, J., Baxter, I., Herein, M., Haszpra, T., et al. (2020). An Internal Atmospheric Process Determining Summertime Arctic Sea Ice Melting in the Next Three Decades: Lessons Learned from Five Large Ensembles and Multiple CMIP5 Climate Simulations. *Journal of Climate*, *33*(17), 7431–7454. https://doi.org/10.1175/JCLI-D-19-0803.1

Wallace, J. M., Fu, Q., Smoliak, B. V., Lin, P., & Johanson, C. M. (2012). Simulated versus observed patterns of warming over the extratropical Northern Hemisphere continents during the cold season. *Proceedings of the National Academy of Sciences*, *109*(36), 14337–14342. https://doi.org/10.1073/pnas.1204875109

Watanabe, M., Shiogama, H., Tatebe, H., Hayashi, M., Ishii, M., & Kimoto, M. (2014). Contribution of natural decadal variability to global warming acceleration and hiatus. *Nature Climate Change*, *4*(10), 893–897. https://doi.org/10.1038/nclimate2355

Weyn, J. A., Durran, D. R., Caruana, R., & Cresswell-Clay, N. (2021). Sub-seasonal forecasting with a large ensemble of deep-learning weather prediction models. *Journal of Advances in Modeling Earth Systems*, *13*(7), e2021MS002502.

Wills, R. C. J., Battisti, D. S., Armour, K. C., Schneider, T., & Deser, C. (2020). Pattern Recognition Methods to Separate Forced Responses from Internal Variability in Climate Model Ensembles and Observations. *Journal of Climate*, *33*(20), 8693–8719. https://doi.org/10.1175/JCLI-D-19-0855.1

Wu, F., Li, W., Zhang, P., & Li, W. (2021). Relative Contributions of Internal Atmospheric Variability and Surface Processes to the Interannual Variations in Wintertime Arctic Surface Air Temperatures. *Journal of Climate*, *34*(17), 7131–7148. https://doi.org/10.1175/JCLI-D-20-0779.1

Wu, T., Hu, A., Gao, F., Zhang, J., & Meehl, G. A. (2019). New insights into natural variability and anthropogenic forcing of global/regional climate evolution. *Npj Climate and Atmospheric Science*, *2*(1), 1–13. https://doi.org/10.1038/s41612-019-0075-7

Xie, S.-P., & Kosaka, Y. (2017). What Caused the Global Surface Warming Hiatus of 1998–2013? *Current Climate Change Reports*, *3*(2), 128–140. https://doi.org/10.1007/s40641-017-0063-0

Ye, K., & Messori, G. (2021). Inter-model spread in the wintertime Arctic amplification in the CMIP6 models and the important role of internal climate variability. *Global and Planetary Change*, *204*, 103543. https://doi.org/10.1016/j.gloplacha.2021.103543

Yu, X., Millet, D. B., Henze, D. K., Turner, A. J., Delgado, A. L., Bloom, A. A., & Sheng, J. (2023). A high-resolution satellite-based map of global methane emissions reveals missing wetland, fossil fuel, and monsoon sources. *Atmospheric Chemistry and Physics*, *23*(5), 3325–3346. https://doi.org/10.5194/acp-23-3325-2023

Zhang, J. H. L., B. Huang, M. J. Menne, X. Yin, A. Sánchez-Lugo, B. E. Gleason, Russell Vose, D. Arndt, J. J. Rennie, C. N. (2019, July 19). Updated Temperature Data Give a Sharper View of Climate Trends. Retrieved May 30, 2023, from http://eos.org/science-updates/updated-temperature-data-give-a-sharper-view-of-climate-trends

Zhang, L. (2016). The roles of external forcing and natural variability in global warming hiatuses. *Climate Dynamics*, *47*(9), 3157–3169. https://doi.org/10.1007/s00382-016-3018-6

Zhang, R., Wang, H., Fu, Q., Pendergrass, A. G., Wang, M., Yang, Y., et al. (2018). Local Radiative Feedbacks Over the Arctic Based on Observed Short-Term Climate Variations. *Geophysical Research Letters*, *45*(11), 5761–5770. https://doi.org/10.1029/2018GL077852

Zhang, R., Wang, H., Fu, Q., & Rasch, P. J. (2020). Assessing Global and Local Radiative Feedbacks Based on AGCM Simulations for 1980–2014/2017. *Geophysical Research Letters*, *47*(12), e2020GL088063. https://doi.org/10.1029/2020GL088063

Zhang, R., Wang, H., Fu, Q., Rasch, P. J., Wu, M., & Maslowski, W. (2021). Understanding the Cold Season Arctic Surface Warming Trend in Recent Decades. *Geophysical Research Letters*, *48*(19), e2021GL094878. https://doi.org/10.1029/2021GL094878